Determination of electron density fluctuation correlation functions via beam emission spectroscopy

1998 Plasma Phys. Control. Fusion 40 1399

(http://iopscience.iop.org/0741-3335/40/7/013)

Plasma Phys. Control. Fusion **40** (1998) 1399–1416. Printed in the UK PII: S0741-3335(98)89907-7

Determination of electron density fluctuation correlation functions via beam emission spectroscopy

S Zoletnik†‡, S Fiedler‡, G Kocsis†, G K McCormick‡, J Schweinzer‡ and H P Winter§

† KFKI-Research Institute for Particle and Nuclear Physics, PO Box 49, H-1525, Budapest, Hungary

‡ Max-Planck-Institut für Plasmaphysik, EURATOM Association, Boltzmannstr. 2, D-85748 Garching, Germany

§ Institut für Allg. Physik, TU Wien, Ass. EURATOM-OEAW, Wiedner Hauptstr. 8-10/134, A-1040 Wien, Austria

Received 4 December 1997, in final form 27 April 1998

Abstract. Measurement of electron density fluctuations in magnetically confined fusion plasmas by the beam emission spectroscopy (BES) method is discussed and an algorithm is given for the correct reconstruction of correlation functions of the electron density fluctuation from measured correlation functions of beam light fluctuations. The technique is generally applicable to all kinds of neutral beams, provided an appropriate model for beam light emission is available and the beam penetration time through the observation volume is shorter than the characteristic times of the plasma turbulence. Light from a 48 keV Lithium beam on W7-AS plasmas is analysed in detail, whereby electron density fluctuations in the scrape-off layer and in the edge plasma are analysed for a low-density electron cyclotron resonance heated (ECRH) heated discharge. Characteristic changes in the autocorrelation function are found at the last closed flux surface. Limitations of the technique are discussed.

1. Introduction

Cross-field transport coefficients in magnetically confined hot plasmas are generally found to be well above neoclassical values [1]. The cause of this anomalous transport is thought to be turbulence both in the edge and core plasma [2, 3]. As turbulence implies fluctuation in plasma parameters, there has been a large interest in determining the characteristics of these fluctuations. The relatively cold and tenuous scrape-off layer (SOL) and, to some extent, the edge plasma can be accessed by solid probes. As a consequence, such probes have been extensively employed in the search for fluctuations in electron density, temperature and electric potential. The frequency spectrum of fluctuations was always found to be a broad one without characteristic frequencies. The spatial structure of perturbations was analysed in detail in the CALTECH [4] and ASDEX [5] tokamaks and in the W7-AS stellarator [6]. Generally the perturbations were found to be randomly appearing structures (eddies) of centimetre size with a lifetime of a few tens of microseconds, aligned to the magnetic field and propagating in the poloidal direction. Radial correlation lengths were also in the centimetre range and no radial propagation was observed in these experiments. On the other hand, measurements with a thermal Li-beam on TEXTOR [7] revealed outward propagating structures in the outer SOL at frequencies below 20 kHz.

0741-3335/98/071399+18$19.50

The core plasma is much less accessible to traditional fluctuation diagnostics, but it is well known from scattering experiments that fluctuations in electron density are present in this region as well [2, 3]. Recently several techniques have been developed to detect fluctuations with appropriate spatial resolution both in the electron density [8, 9] and the electron temperature [10]. For a review of fluctuation measurements in magnetically confined fusion plasmas see [2, 3, 11].

Experimental results, both in the SOL and in the core plasma, indicate that the perturbations responsible for anomalous transport are most probably the ones with long wavelength, that is of centimetre structure size on current machines. It has also been shown that by observing light emitted by a neutral beam traversing the hot plasma, one can gain spatially and temporally well resolved information on electron density perturbations in this important long-wavelength range [12]. Different experimental arrangements have been discussed in the literature using accelerated beams for core plasma measurements [13, 14] and thermal beams for the SOL [15]. In both cases the technique proved to be adequate, but in several cases the exact interpretation is made difficult by the fact that light emitted at a certain position in the plasma is affected by the entire plasma layer between the point in question and the plasma boundary. This effect was investigated by computer simulations both for an accelerated H-beam [16] and a thermal Li-beam [15]. This demonstrated that under certain conditions parameters of the local electron density fluctuations could be calculated from fluctuations in the beam light emission.

In this paper we present a general method for the reconstruction of correlation functions of electron density fluctuations from the measured correlation functions of beam light emission. The method is general in the sense that it can be applied for any kind of beam experiment, provided: (a) an appropriate model is available for the light emission as a function of electron density and other plasma parameters and (b) the beam penetration time through the observation volume is shorter than the characteristic times of the plasma turbulence. Here the method is applied for measurements with a 48 keV Li-beam [17, 18] on the W7-AS stellarator. This diagnostic can access the whole SOL together with a substantial fraction of the core plasma for low-density discharges. Capabilities and limitations of the measurement are discussed. First results for low-density ECRH heated plasmas are presented.

2. General considerations

Let us consider a beam of accelerated atoms penetrating the plasma. The key parameter determining the rate of atomic physics processes in the beam is the plasma electron density. Other quantities such as electron temperature, Z_{eff}, etc affect the rates as well but their importance is usually subordinate. For the specific case of the W7-AS Li-beam diagnostic their effect is known to be small. Thus, electron temperature and Z_{eff} profiles, taken from other diagnostics, are assumed to be constant in time in the treatment described later. This way, light emission at a given Z beam coordinate is a complicated nonlinear function of the whole electron density profile outside Z. With knowledge of T_{e}, Z_{eff} and the atomic physics processes taking place in the beam, one can deduce the electron density profile corresponding to a measured light profile [19]. As the numerical procedure for this reconstruction inverts an integral transformation it is rather sensitive to errors in the light measurement. This fact restricts the applicability of the unfolding method to measurements where the integration time of the light detectors is long enough to keep photon statistical noise at an acceptable level, typically below 10%. Increasing the temporal resolution of the measurement, and thereby the noise level, leads to a breakdown of the density reconstruction method.

On the other hand, statistical properties, such as correlation functions between two light signals can be determined with high accuracy for repetitive phenomena if the light signals are sampled over a sufficiently long period. Naturally, the correlation functions determined this way may be considerably different from the correlation functions of the electron density fluctuations, as the beam light is not a local function of plasma electron density. Correlations between two different places along the beam are obviously different for beam light and electron density, but even autocorrelation functions (correlation at one place as a function of time delay) are distorted.

Similarly, correlation functions of beam light fluctuations are different from correlation functions of density fluctuations using a broad atomic beam when trying to determine correlation functions of density fluctuations between points displaced perpendicularly relative to the beam axis [20]. As the beam usually penetrates the plasma along a minor radius a wide beam allows for either toroidal or poloidal correlation measurements. Problems associated with spatially broad beams are outside the scope of the present paper, but a numerical method similar to the one to be described in the next section should be able to unfold the original correlation functions of electron density fluctuations.

3. Description of the method

By modelling the population of the atomic levels of beam particles interacting with an ambient hot plasma, one can calculate the light intensity distribution $S(Z, t)$ arising from an arbitrary electron density distribution $n_e(Z, t)$

$$S(Z, t) = \mathcal{F}\{n_e(Z', t)\} \qquad 0 \leqslant Z' \leqslant Z. \tag{1}$$

Here Z denotes the coordinate along the beam starting at the plasma edge and increasing towards the plasma centre. Since the beam penetration time through the observation volume is much shorter than the time resolution of the measurement it is considered to be instantaneous. The temporal behaviour of the electron density distribution can be written as a sum of two terms, a time-independent (average) and a time-dependent perturbative part

$$n_e(Z, t) = n_e^0(Z) + \tilde{n}_e(Z, t). \tag{2}$$

If the perturbations are small relative to the average electron density for all values of Z, one can linearize the transformation $\mathcal{F}$ in equation (1) as

$$S(Z, t) = S^0(Z) + \tilde{S}(Z, t) \qquad S^0(Z) = \mathcal{F}\{n_e^0(Z')\}$$
$$\tilde{S}(Z, t) \approx \int_0^Z \tilde{n}_e(Z', t) h(Z, Z')\, \mathrm{d}Z' \tag{3}$$

where $h(Z, Z')$ is a transfer function describing the effect of a small density change at Z' on the light signal at Z. One should have in mind, that the function $h(Z, Z')$ depends on the average electron density distribution $n_e^0(Z)$. The validity of this linear approximation was investigated by numerical simulations for typical W7-AS density profiles (peak n_e between 1×10^{19} and 10×10^{19} m^{-3}). It was found that the deviation between the linear and the detailed light calculation is well below 1% of the total beam light even if the edge density perturbations reach 100%. The linearized treatment breaks down only if perturbations in the density profile with more than 10% amplitude appear in the region where the beam is substantially attenuated. For at least low- and medium-density (peak $n_e \leqslant 3 \times 10^{19}$ m^{-3}) discharges on W7-AS this is typically not the case. However, in special cases (e.g. if global Alfvén eigenmodes (GAE) are present in the plasma) fluctuations might have too high an amplitude to fulfil the above linearity condition. A linear relationship between edge electron

density fluctuations and corresponding beam light intensity fluctuations was also pointed out for an accelerated H-beam in [16].

The crosscorrelation function C^S (without normalization) between the light emission at Z_1 and Z_2 at time delay τ is defined as

$$C^S(Z_1, Z_2, \tau) = \frac{1}{T}\int_0^T \tilde{S}(Z_1, t)\tilde{S}(Z_2, t+\tau)\,\mathrm{d}t \tag{4}$$

where T is the total measurement time. The density crosscorrelation function C^n is defined similarly as

$$C^n(Z_1, Z_2, \tau) = \frac{1}{T}\int_0^T \tilde{n}_\mathrm{e}(Z_1, t)\tilde{n}_\mathrm{e}(Z_2, t+\tau)\,\mathrm{d}t. \tag{5}$$

As the fluctuation power is given by the autocorrelation at zero time delay $C(Z, Z, 0)$, the normalized crosscorrelation functions $\overline{C}$ can be expressed as

$$\overline{C}(Z_1, Z_2, \tau) = \frac{C(Z_1, Z_2, \tau)}{\sqrt{C(Z_1, Z_1, 0)C(Z_2, Z_2, 0)}}. \tag{6}$$

Equation (6) is somewhat different from the usual normalization of the correlation function as the signal power at $Z = Z_2$ is calculated in the time interval $(0, T)$ instead of $(\tau, T+\tau)$. If the density fluctuation originates from a stationary process and the time interval T is sufficiently long, the difference is small. However, the correlation functions normalized this way are not strictly confined between -1 and $+1$. Even so, equation (6) has the advantage that normalization can be done using exclusively the unnormalized correlation functions.

Substituting the linearized approximation of the light signal from equation (3) into equation (4) and using equation (5), one arrives at a linearized transformation between the crosscorrelation functions of the density and light perturbations

$$C^S(Z_1, Z_2, \tau) = \int_0^{Z_1}\int_0^{Z_2} h(Z_1, Z')h(Z_2, Z'')C^n(Z', Z'', \tau)\,\mathrm{d}Z'\,\mathrm{d}Z''. \tag{7}$$

For every τ equation (7) describes the same integral transformation from the two-dimensional density crosscorrelation function C^n to the light crosscorrelation function C^S. To reconstruct $C^n(Z_1, Z_2, \tau)$ one needs the whole $C^S(Z', Z'', \tau)$ profile at the same τ. The transformation is identical and independent for different delay times.

In an actual measurement one measures the light intensity at a finite N_S number of Z^S points and as a consequence a number of N_S^2 values for C^S become known. The electron density distribution for the calculations is defined at N_n number of Z^n points along the beam, which need not be the same points where the light signals are measured. Between these points the electron density distribution is linearly approximated. This treatment is identical to a series expansion of $\tilde{n}_\mathrm{e}(Z, t)$ in the form of

$$\tilde{n}_\mathrm{e}(Z, t) = \sum_{i=1}^{N_n} P_i(t)\, f_i(Z) \tag{8}$$

where $f_i(Z)$ are the base functions of the series expansion $f_i(Z_j^n) = \delta_{ij}$ and linearly change between the Z^n points. This way $\tilde{n}_\mathrm{e}(Z_i^n) = P_i$. Two more points are taken at the ends of the electron density profile, where $\tilde{n}_\mathrm{e}$ is set to zero. Substituting equation (8) into the linearized expression for $\tilde{S}(Z, t)$ in equation (3) one arrives at a linear transformation between the

$P_j(t)$ parameters of the density profile perturbation and the measured light perturbations

$$\tilde{S}(Z_i^S, t) = \tilde{S}_i(t) = \sum_{j=1}^{N_n} M_{ij} P_j(t) \tag{9}$$

$$M_{ij} = \int_0^{Z_i^S} f_j(Z') h(Z_i^S, Z')\, \mathrm{d}Z'. \tag{10}$$

The M_{ij} matrix is the discretized counterpart of the $h(Z, Z')$ transfer functions. M_{ij} is calculated by adding a small amplitude $\epsilon f_j(Z)$ perturbation to the average density profile and calculating the change in the light signal at Z_i^S. Using the expression for the crosscorrelation functions in equations (4) and (5) one arrives at the discretized form of equation (7)

$$\begin{aligned} C^S(Z_k^S, Z_l^S, \tau) = C_{kl}^S(\tau) &= \sum_{i=1}^{N_n} \sum_{j=1}^{N_n} M_{ki} M_{lj} \frac{1}{T} \int_0^T P_i(t) P_j(t+\tau)\, \mathrm{d}t \\ &= \sum_{i=1}^{N_n} \sum_{j=1}^{N_n} M_{ki} M_{lj} C_{ij}^n(\tau) \end{aligned} \tag{11}$$

or in matrix notation

$$\mathbf{C}^S = \mathbf{M}\mathbf{C}^n\mathbf{M}^{\mathrm{T}}. \tag{12}$$

In this last expression and in all the following ones the dependence of the correlation matrices on τ is not indicated as the transformation is independent of it. Rearranging the elements of the $\mathbf{C}^n$ and $\mathbf{C}^S$ matrices into N_n^2 and N_S^2 element vectors $\vec{C}^n$ and $\vec{C}^S$, respectively, equation (12) can be transformed into the form

$$\vec{C}^S = \hat{\mathbf{M}}\vec{C}^n \tag{13}$$

where $\hat{\mathbf{M}}$ is a $(N_S^2 \times N_n^2)$ matrix. If N_s is equal to N_n then in theory it would be possible to solve equation (13) by inverting matrix $\hat{\mathbf{M}}$. In practice, this approach never works as the problem is so ill-conditioned that even small measurement errors generate heavily oscillating density crosscorrelation functions. One can avoid this behaviour by applying one of the following methods.

(i) Keep N_n well below N_S and minimize

$$(\vec{C}^S - \hat{\mathbf{M}}\vec{C}^n)^2. \tag{14}$$

This treatment can be adequate if the number of measurement points is high and the shape of the density crosscorrelation functions C^n can be adequately represented by the decreased number of N^n points.

(ii) Use a regularization method as it is performed in computer tomography and find a solution which fits the measured light crosscorrelation function within error bars and is otherwise 'smooth'.

As (i) strongly reduces the spatial resolution of the calculation it is not discussed here. Instead a fast and effective regularization technique [21] is applied which minimizes

$$H(\vec{C}^n) = \int\int \left[\left(\frac{\mathrm{d}C^n(Z', Z'')}{\mathrm{d}Z'} \right)^2 + \left(\frac{\mathrm{d}C^n(Z', Z'')}{\mathrm{d}Z''} \right)^2 \right] \mathrm{d}Z'\, \mathrm{d}Z'' = \vec{C}^n \hat{\mathbf{H}} \vec{C}^n \tag{15}$$

with the constraint

$$\chi(\vec{C}^n) = \frac{1}{N_S^2} \sum_{i=1}^{N_S^2} \frac{[(\vec{C}^S)_i - (\hat{\mathbf{M}}\vec{C}^n)_i]^2}{\sigma_i^2} = 1. \tag{16}$$

σ_i denotes the experimental errors of the light signal crosscorrelations $\vec{C}^S$. The elements of the matrix $\hat{\mathbf{H}}$ depend only on the position of the Z_i^n points and can be calculated analytically using the series expansion of $\tilde{n}_e(Z)$ in equation (8). In other words, this method finds a solution which is in a statistical sense correctly close to the measured light crosscorrelation functions (equation (16)) and smooth in the sense of equation (15).

For this treatment one needs a correct error estimate of the light crosscorrelation function. This can be done by dividing the integration time interval $(0, T)$ in equation (4) (observation time) into smaller subintervals. The crosscorrelation function is then calculated in each of these intervals. The mean of these crosscorrelation values gives the final crosscorrelation, while the standard deviation of them divided by the square root of the number of intervals gives the error estimate. This estimation assumes that statistical fluctuations of the correlation values are dominated by photon statistics and not by statistics of the electron density fluctuations. If this assumption is not true, then the error estimate can be too high and the reconstruction algorithm will tend to underestimate electron density correlations.

Equation (15) is solved under the constraint of equation (16) as described in [21]. The whole procedure (calculation of the light crosscorrelation functions and their error estimates, solution of equations (15) and (16)) is done independently for all τ delay times. It should be noted that if the resolution of the expansion of the density crosscorrelation function (equation (8)) is too rough or the error estimates are too low, no solution exists to the equations.

As detailed in [21] the above described problem is solved by iteratively finding a $\hat{\mathbf{T}}$ matrix which transforms the measured $\vec{C}^S$ crosscorrelation values to the desired $\vec{C}^n$ values as

$$\vec{C}^n = \hat{\mathbf{T}}\vec{C}^S. \tag{17}$$

This linear expression gives us the possibility to calculate a statistical error estimate of the elements of $\vec{C}^n$. Assuming a statistically independent scatter of the elements of $\vec{C}^S$ the statistical error of the calculated electron density crosscorrelation vectors is

$$\sigma_i^n = \sqrt{\sum_{j=1}^{N^S} \hat{T}_{ij}^2 \sigma_j^2}. \tag{18}$$

One problem remains to be considered. By selecting a long integration time interval T the error of the light crosscorrelation function $C^S(Z_1, Z_2, \tau)$ can be reduced arbitrarily. The only exception is for $\tau = 0$ and $Z_1 = Z_2$ (autocorrelation at zero time delay). At this point the effect of photon statistical noise cannot be avoided. If one uses a finite f_{max} bandwidth amplifier for the light signal measurement, then the photon noise has an effect not only at $\tau = 0$ but roughly for $\tau < 1/f_{max}$. The contribution of photon noise to the crosscorrelation functions is an additional effect which is not included in this treatment, hence it should be eliminated before applying the reconstruction method. The simplest way of handling this problem is to leave out those τ values where the crosscorrelation is affected by photon noise. However, this means that $C^n(Z, Z, 0)$ will be unknown and thus the normalized crosscorrelation functions (see equation (6)) cannot be calculated.

If the frequency spectrum of the density fluctuations is limited to much lower frequencies than the sampling frequency of the signals, then at around $\tau = 0$ the crosscorrelation function (without photon noise) changes slowly. This fact makes it possible to remove the photon noise contribution from the crosscorrelation functions by approximating it around $\tau = 0$ as it is shown in figure 1 (full curve). With this technique the normalized crosscorrelation

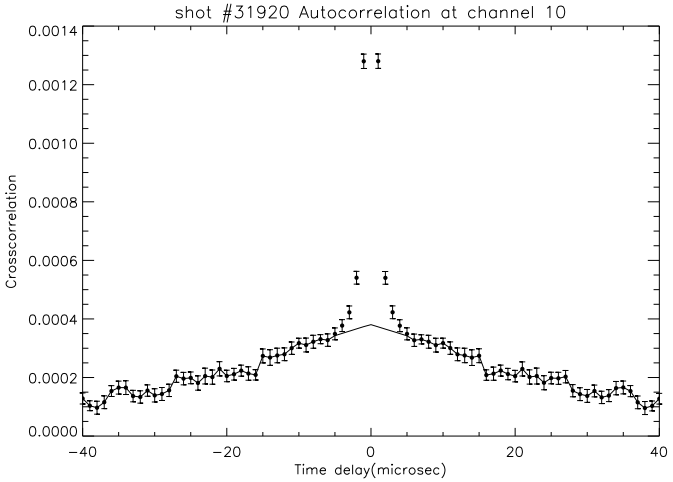

Figure 1. Experimentally measured autocorrelation function. The full curve represents a linear extrapolation of the curve around $\tau = 0$ based on the values in the interval $5 < \tau \leqslant 15$.

functions can be calculated, but some side effects appear, for example the normalized autocorrelation function can sometimes rise above one.

Another possibility for the treatment of photon statistical noise is to leave out the contribution of the autocorrelations in the sum of equation (16). Of course, in this case N_S^2 in the nominator should be substituted by the real number of terms in the sum. This way reconstruction is possible even if the frequency of the electron density fluctuations is comparable to the sampling frequency of the measurement. However, this method introduces problems if the crosscorrelation of the light fluctuations changes on a spatial scale comparable to the spatial resolution of the experiment.

4. Numerical tests of the method

The numerical method described in section 3 is tested using computer generated signals. Properties of these artificial signals (e.g. the number of samples, photon statistics) were set to about the same values as in the experiments. An average electron density profile ($n_e^0(Z_i^S)$, $N_S = 24$) was taken from a plasma discharge and computer generated density fluctuations were added to it in the following way: a 200 000 element random vector was generated and smoothed with a boxcar smoothing algorithm. This 'density fluctuation signal' was shifted in time, multiplied by an amplitude factor and added to each of the 24 average density values. The amplitude and time shift were changed from channel to channel. The smooth length (boxcar size), amplitudes, and time delays were selected in such a way that the correlation functions of the simulated light fluctuations were similar to the ones observed experimentally. Parameters of the simulation are shown on figure 2.

The light signal was calculated for each of the 200 000 density profiles using the linear approximation of equation (9). In order to simulate photon statistics each of the 24 simulated signals at each of the 200 000 time points were determined by generating a random number with Poisson statistics having a mean value proportional to the light intensity. The root-mean-square (RMS) deviation of the signals due to statistics was set to be equal to the RMS value of the photon statistical noise observed in the experiment.

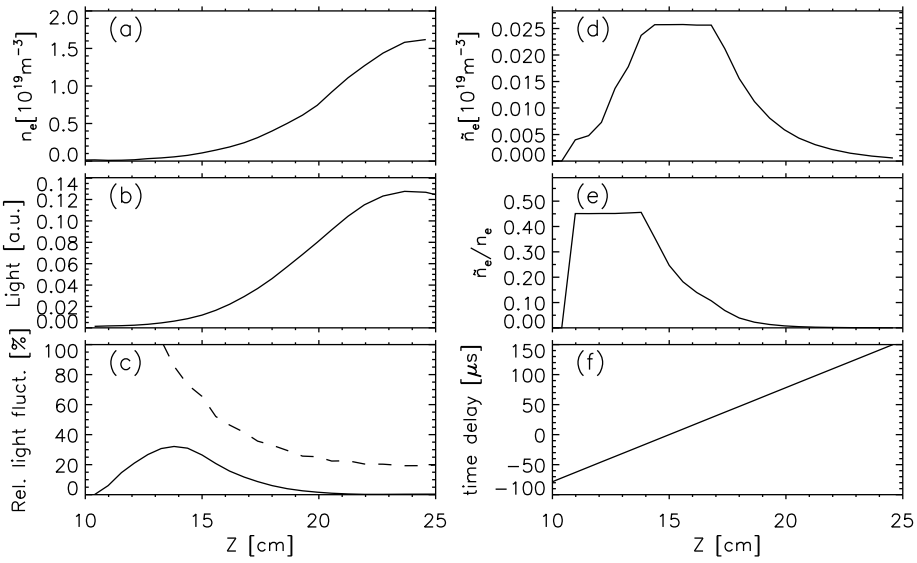

Figure 2. Parameters of simulated density fluctuations: (a) mean electron density profile, (b) mean light profile, (c) percentage RMS fluctuation of simulated light signals due to density fluctuations (——) and photon statistics (– – –), (d) electron density fluctuation amplitude, (e) relative electron density fluctuation amplitude, and (f) profile of fluctuation time delay.

The simulated signals generated in this way were processed with the algorithm described in section 3. The computer program was written in the IDL data processing language. The density crosscorrelation functions were reconstructed using $N_n = 15$ points equidistantly arranged with a distance of 1 cm. Each τ time delay was processed independently. Calculation time for a single delay time was approximately 30 s both on a silicon graphics workstation (MIPS R4400 150 MHz processor) and an IBM PC compatible (Pentium 166 MHz processor under a Linux 2.0.0 operating system).

To remove photon statistical noise generated autocorrelation around $\tau = 0$ the autocorrelation functions were extrapolated in the vicinity of $\tau = 0$ as described at the end of section 3. The time resolution of the crosscorrelation functions was reduced from 1 μs (resolution of the measured or simulated signals) to 11 μs. This way the crosscorrelation at τ actually means the average in the $\tau = [\tau - 5\ \mu\text{s}, \tau + 5\ \mu\text{s}]$ interval. For reference, crosscorrelation functions of the computer generated electron density fluctuations were calculated the same way, but no extrapolation was done around $\tau = 0$.

Figure 3 plots the result of a typical calculation for a low electron density plasma at $\tau = 0$. One can clearly see how nearly the original width of the crosscorrelation functions is reproduced by the reconstruction algorithm. A cut of figure 3 is plotted on figure 4. One can see that the light crosscorrelation function corresponding to the reconstructed density crosscorrelation function (i.e. $\hat{\mathbf{M}}\vec{C}^n$ in equation (16)) fits the crosscorrelation values of the 'measured' light within the error bars, as it is required by the $\chi(\vec{C}^n) = 1$ constraint. This is not true if one compares the original density crosscorrelation values with the reconstructed curve. The fit is not ideal, as the photon noise in the 'measurement' hides part of the correlation information. Moreover, the spatial resolution of the reconstructed crosscorrelation functions is less than that of the original ones and thus no perfect agreement is expected between the original and reconstructed density correlations. If the photon noise

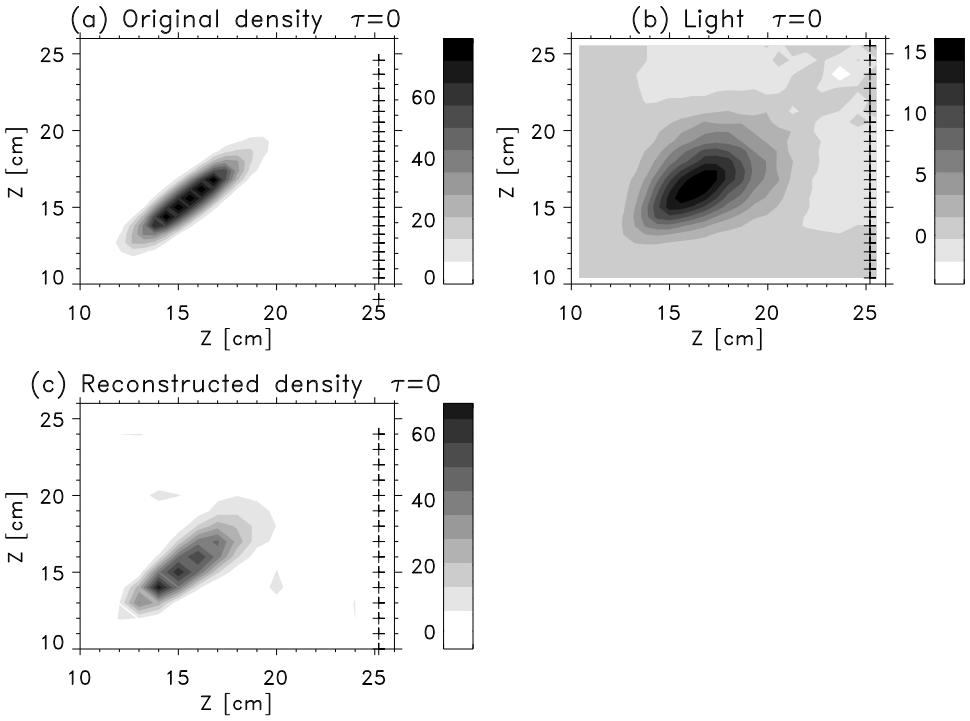

Figure 3. Correlation functions $C(Z, Z, 0)$ in the simulation for (a) original simulated density, (b) simulated light and (c) reconstructed density. The crosses next to the right edge of each figure show the points, where the functions are calculated. (Z_i^S for the correlation functions of light fluctuations and Z_i^n for the reconstructed correlation functions of density fluctuations.) The colour scales of the two density plots are the same.

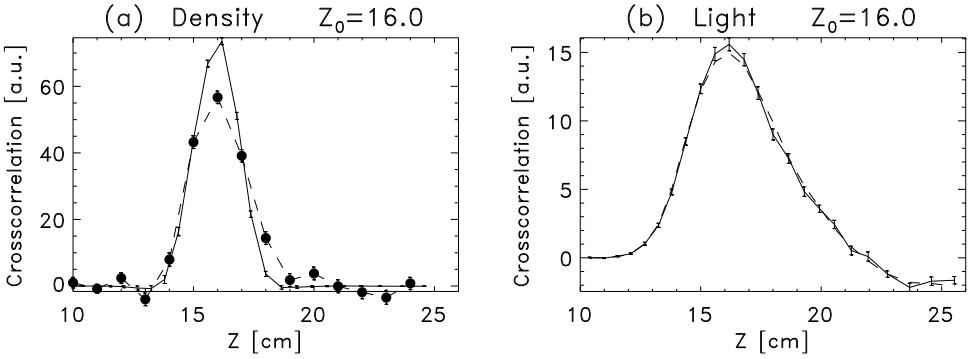

Figure 4. Crosscorrelation functions $C(Z, Z_0, 0)$ in the simulation, i.e. cuts of figure 3. (a) Original simulated density (——) and reconstructed density (– – –), (b) simulated light and light corresponding to reconstructed density (– – –).

level is decreased (or if the measurement time interval is increased) the fit becomes closer. The algorithm could determine the density crosscorrelation function, with approximately 1 cm spatial resolution although the lifetime of the Li (2p) atomic level introduces a spatial smoothing in the light emission along the beam with an e-folding length of 3.1 cm [22].

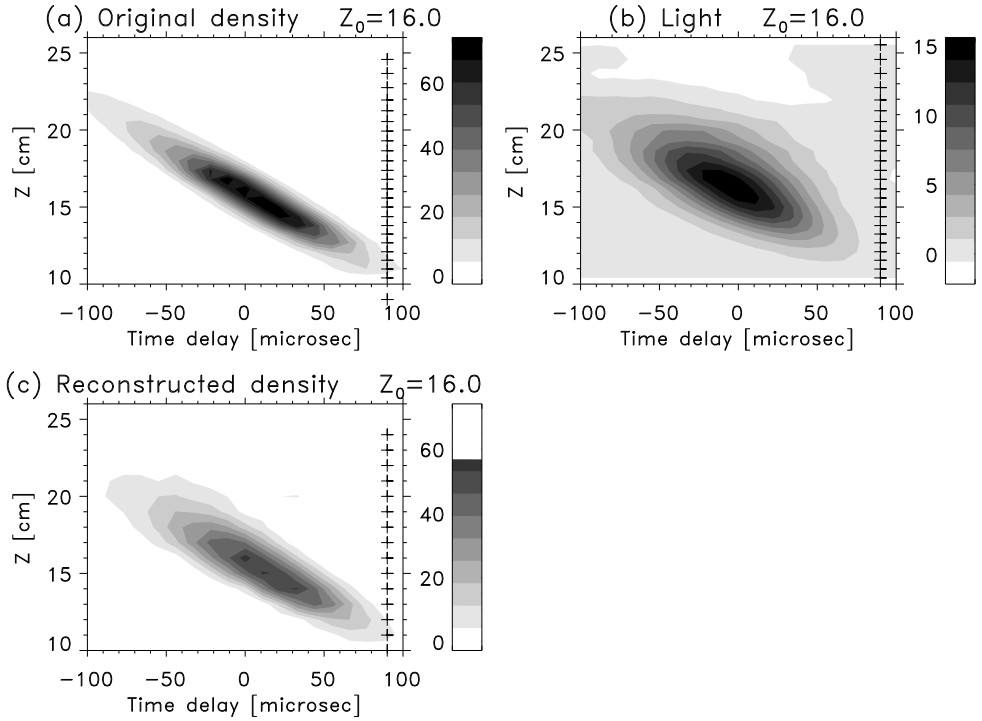

Figure 5. Crosscorrelation functions $C(Z_0, Z, \tau)$ in the simulation for (a) original simulated density, (b) simulated light and (c) reconstructed density. More explanation at figure 3.

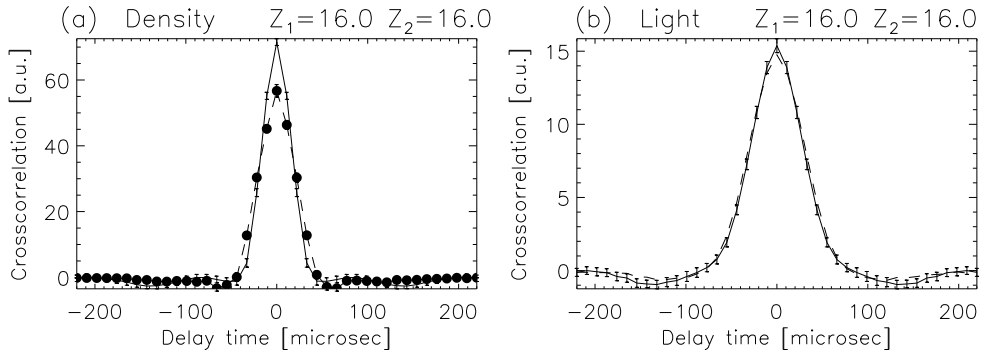

Figure 6. Autocorrelation functions $C(Z_0, Z_0, \tau)$ in the simulation, i.e. cuts of figure 5. (a) Original simulated density (——) and reconstructed density (– – –), (b) simulated light and light corresponding to reconstructed density (– – –).

Figure 5 shows time–space correlation functions from a compilation of results obtained at independent τ time delays. The reconstructions at different time delays fit together well and the propagating nature of the fluctuations is clearly resolved. The autocorrelation function at $Z_0 = 16$ cm (horizontal cut of figure 5) is plotted in figure 6.

The same calculation was performed for different absolute values of the electron density profile. For these tests the electron density profile in figure 2 was multiplied by factors

ranging from two to four and the amplitude of the electron density fluctuations was multiplied by the same factors, in order to keep the percentage electron density fluctuations constant. Although the shape of the light crosscorrelation functions changed the calculation could unfold the original crosscorrelation functions of the electron density fluctuations. An example is shown for a peak electron density value of 6.4×10^{19} m^{-3} in figure 7.

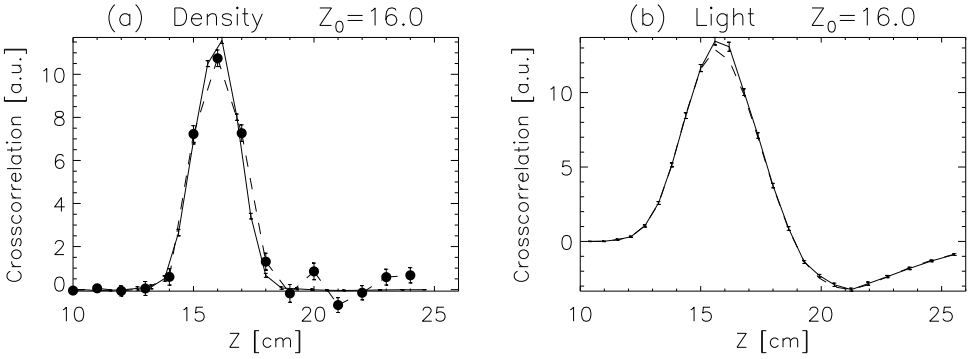

Figure 7. Crosscorrelation functions $C(Z, Z_0, 0)$ in the simulation for a mean electron density four times higher than the one shown in figure 2. (a) Original simulated density (——) and reconstructed density (– – –), (b) simulated light and light corresponding to reconstructed density (– – –).

4.1. Sensitivity to parameter changes

To test the sensitivity of the reconstruction to different parameters the same computer generated test signals were used, but the **M** matrix of the reconstruction was calculated using different electron temperature, density and Z_{eff} profiles.

By modifying the local electron temperatures by factors ranging from 0.5 to 3, the correlation length of the reconstructed electron density fluctuation crosscorrelation functions changed much less than the resolution of the reconstruction (1 cm). The reconstructed profile of the fluctuation amplitude (square root of autocorrelation values at $\tau = 0$) changed by about 30%. Reconstructed fluctuation amplitudes always underestimated the actual fluctuation amplitudes. Similar results were obtained when the Z_{eff} profile was changed. The correlation length did not change significantly, but the fluctuation amplitude profile changed slightly in the order of some tens of percents.

The mean density used in the reconstruction is calculated from the measured mean light profile and represents the real local electron density distribution along the beam. However, wrong input parameters ($T_{\text{e}}(Z)$, $Z_{\text{eff}}(Z)$) to the calculation might distort the density profile in a way that the calculated light profile fits the measured one. This means that the rate of the atomic physics processes determining the beam light emission will equal the real ones, but, for example, at another combination of electron density and electron temperature. As the $h(Z, Z')$ transfer function is determined by the rate of the atomic physics processes and not by the electron density itself, it should be independent of these types of errors.

4.2. Limitations of the Li-beam fluctuation measurement

Limitations in spatial, temporal and amplitude resolution of fluctuation measurements with the W7-AS Li-beam diagnostic are discussed in this section. Although other beams and

experimental set-ups may lead to different limits, the general considerations should hold for all BES experiments.

Spatial resolution along the beam is determined by two parameters, namely resolution of the detection system and the length associated with the relaxation time of beam atomic physics processes. It was shown in the previous section that a correlation length of approximately 1 cm can be reconstructed by the unfolding procedure although the lifetime of the Li (2p) atomic level corresponds to a length of about 3 cm. In theory, the unfolding procedure should work for even shorter correlation length, but this would necessitate higher spatial resolution in the experiment and would certainly increase the noise sensitivity of the method. Thus, the resolution of 1 cm is a practical lower limit. On the other hand, the finite width of the beam introduces a spatial integration perpendicular to its axis. As a consequence, the sensitivity to perturbations having a poloidal size less than the beam diameter is rather low. As the poloidal and radial correlation lengths of electron density fluctuations are usually close to each other both in the SOL [4, 5] and in the core plasma [9] there is no need to have a finer radial resolution than the beam diameter.

The temporal resolution is largely determined by photon statistics, the amplitude of the density fluctuations in question and the total measurement time. For a total measurement time of a few hundred milliseconds, 1 mA Li-beam current and 10% density fluctuation at the last closed flux surface (LCFS) the maximum temporal resolution of the crosscorrelation functions is about 10 μs. At this resolution the amplitude of the fluctuations in the beam light signals due to density fluctuations is a few times below the photon noise level. Using a higher efficiency detection system (e.g. [23]) and higher beam current, the photon noise level could possibly be decreased and as a consequence the time resolution of the crosscorrelation functions could be improved, or alternatively the measurement could be made sensitive to lower amplitude (few per cent) density fluctuations.

The fluctuations around the LCFS are of sufficiently high amplitude to be detected by the Li-beam diagnostic. In contrast to this region, in the core plasma the density fluctuation level is expected to be around 1%, which suggests with some improvements the diagnostic could successfully investigate core plasma fluctuations as well. However, the situation, at least for the 48 keV Li-beam is not so promising, as deeper in the plasma the light of the beam becomes more and more insensitive to density fluctuations. This effect was investigated by computer simulation. A density profile was taken from a plasma discharge and a 2 cm FWHM Gaussian shape perturbation was added to it centred at position Z. The amplitude of the perturbation was 1% of the local density at Z. The percentage increase in the Li-beam light at Z in response to this bump is plotted as a function of the bump position Z in figure 8. The procedure was repeated after multiplying the density profile by 2, 3 and 4. The figure clearly shows how the response drops in the core plasma, and that the drop is much more pronounced at higher electron densities. Due to this fact, low-amplitude core plasma fluctuations cause undetectably low-level fluctuations in beam light emission. This behaviour is caused by the attenuation of the beam due to ionization and thus a higher ionization potential of the beam particles (e.g. H-, He-beam) should improve the sensitivity to core plasma fluctuations.

5. Experimental results

The first experimental results obtained at the W7-AS stellarator using the discussed processing technique are described in this section. The arrangement of the Li-beam diagnostic on W7-AS is shown in figure 9. The experiments were performed in low-density peak $n_e \approx 1.5 \times 10^{19}$ m^{-3}, 70 GHz ECRH heated hydrogen discharges with $B_t = 1.25$ T

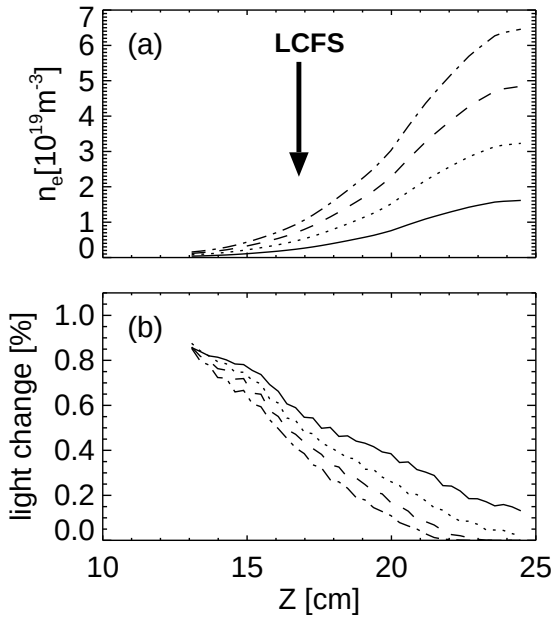

Figure 8. Relative change of the beam light in response to a 1%, 2 cm wide density bump at different places along the beam, for different density distributions shown in (a). See text for more explanation.

toroidal magnetic field and $\iota_a = 0.345$ edge rotational transform. A steady-state 200 ms time interval was selected in the discharges and signals of the outermost 24 photomultipliers (out of the 28 looking at the Li-beam) were digitized at a 1 MHz sampling rate. The resulting 200 000 data points per channel had photon statistics similar to the simulated signals which were used for testing the numerical reconstruction method. Identical pairs of discharges were compared, one with Li-beam and one without, in order to check that the detected light fluctuations come from the Li (2p) line radiation of the beam and not from fluctuations in the background light, which was typically 10 times less intensive than the Li (2p) line radiation.

Crosscorrelation functions were calculated in a delay time range of a few hundred microseconds around zero, but only the $\tau = [-150\ \mu\text{s}, 150\ \mu\text{s}]$ range showed correlations significantly different from zero. Part of a typical correlation function is shown in figure 1. The mean electron density profile along the Li-beam was calculated the standard way [17, 22] using all of the 28 light signals sampled at a 5 kHz sampling rate. The electron temperature profile was obtained from electron cyclotron emission (ECE) measurements.

For the reconstruction of the correlation functions of electron density fluctuation, the light correlation functions were calculated with 11 μs time resolution as described in section 4. For the handling of photon statistical noise, both methods described in section 3 were applied, but in both cases the calculated errors of the reconstruction (and the scattering of the reconstructed values) at $\tau = 0$ were much higher than at $\tau \neq 0$. This is most probably caused by high-frequency (short correlation time) fluctuations inside the LCFS. Indeed, the light crosscorrelation functions a few centimetres inside the LCFS show a 10–20 μs wide peak around $\tau = 0$, but the peak amplitude is only a few times higher than the error bars.

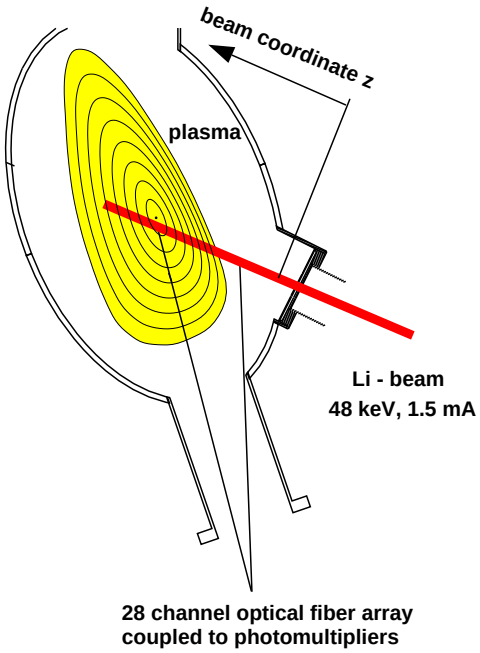

Figure 9. Experimental set-up of the Li-beam diagnostic on W7-AS.

This fact produces higher error bars for the reconstruction at $\tau = 0$ and hence reconstructed correlation values at $\tau = 0$ are omitted in the figures. At the same time this means that normalized correlation functions cannot be calculated from equation (6). Nevertheless basic properties of the low-frequency ($\leqslant$100 kHz) electron density fluctuations can be analysed even in this case.

Figure 10 shows τ–Z plots of reconstructed electron density crosscorrelation functions $C^n(Z_0, Z, \tau)$ for three different Z_0 reference points. Autocorrelation functions with error bars at approximately the places of the reference points are given in figure 11. In these figures the following observations can be made.

(a) Outside the LCFS (i.e. in the SOL) (figure 10(c)) the fluctuations show outward propagation. This is indicated by the fact that at positions inside the reference point maximum correlation occurs at negative delay times, while for points outside the reference point for positive delay times. The full curve approximately shows the shift in maximum correlation as a function of distance from the reference point. The slope of this curve indicates that the propagation velocity is approximately about 5×10^4 cm s^{-1}. This propagating structure is found only in the SOL and not inside the LCFS, as it can be seen in figure 10(b).

(b) Inside the LCFS (figure 10(a)) the fluctuations seem to have an inward propagating character but it is not so clear as outward propagation for the SOL.

(c) The autocorrelation functions in figure 11 have significantly different character in the SOL, at the LCFS and inside the LCFS. In the SOL the correlation time is about 30–40 μs, while at the LCFS it is only about 10 μs. Inside the LCFS the correlation time increases again to about 30–40 μs, but a negative correlation appears in the autocorrelation function between 60–100 μs.

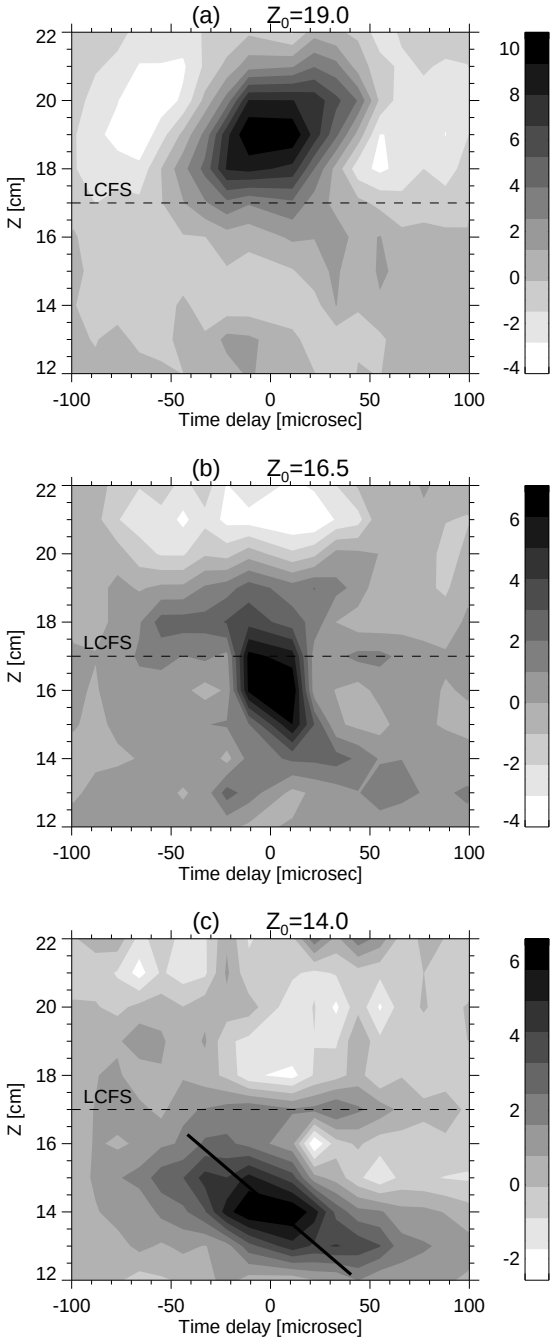

Figure 10. Reconstructed time–space crosscorrelation functions (without normalization) of electron density fluctuations. (a) Reference point 2 cm inside the LCFS, (b) reference point at the LCFS, (c) reference point 3 cm outside the LCFS. The full line indicates approximately how maxima of the crosscorrelation functions (cut at fixed Z) shift as they move away from the reference point.

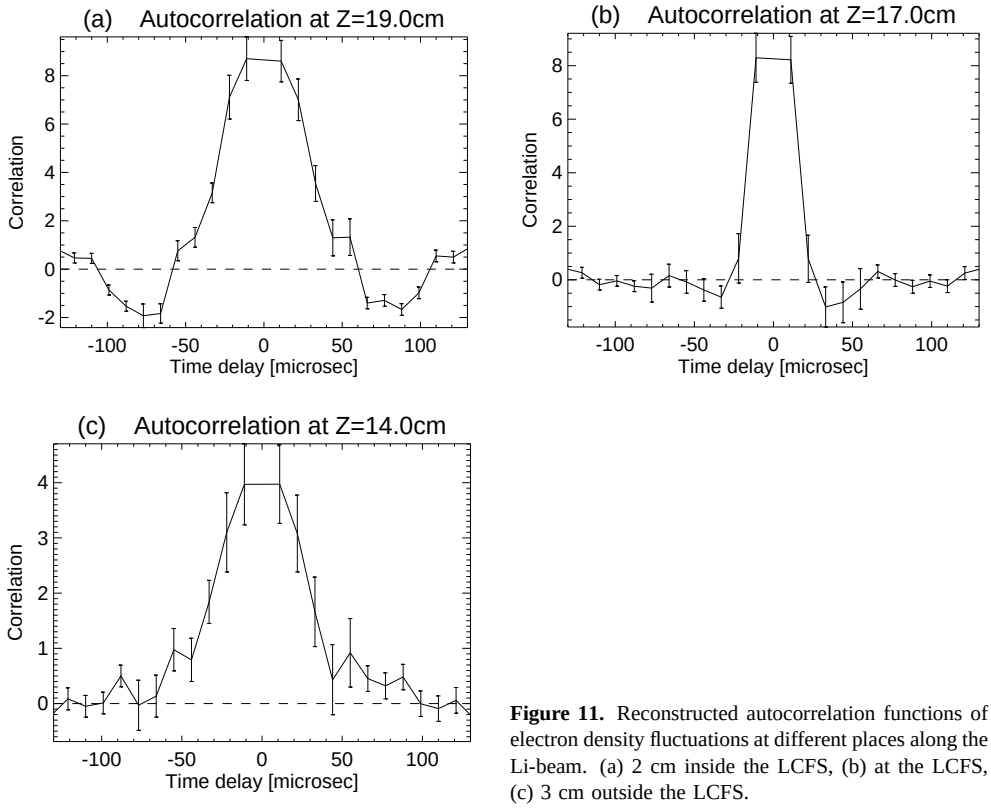

Figure 11. Reconstructed autocorrelation functions of electron density fluctuations at different places along the Li-beam. (a) 2 cm inside the LCFS, (b) at the LCFS, (c) 3 cm outside the LCFS.

6. Discussion

Previous measurements with H_α and Langmuir probe diagnostics on ASDEX and W7-AS [5, 6] showed that the dominant electron density fluctuations in the SOL and around the LCFS have several centimetres poloidal wavelength and a few tens of microseconds correlation time. Hence they should be well detectable with the approximately 1 cm diameter beam of the Li-beam diagnostic. Indeed, the first experimental results described in section 5 show autocorrelation times between 10–50 μs, which agree well with the H_α and Langmuir probe measurements. It should be noted that our results indicate that the autocorrelation time depends strongly on the radial position. The H_α measurements showed a wavelike structure in the poloidal direction whose poloidal propagation causes a somewhat periodic autocorrelation function. As the Li-beam measurement has no poloidal resolution, the wave-like feature could manifest itself only in a periodic autocorrelation function. In the SOL there is no sign of periodicity, but inside the LCFS negative correlations do appear in the autocorrelation function between 50–100 μs which is again in good agreement with H_α results. As the poloidal propagation velocity is known to depend strongly on the radial position, the non-periodic autocorrelation functions in the SOL could be caused by perturbations with slow poloidal propagation velocities and lifetimes shorter than the time period in the autocorrelation function.

In the SOL the perturbations seen by the Li-beam diagnostic propagate outwards. Similar outward propagating structures were observed in the SOL of TEXTOR [7] in the low-frequency (<20 kHz) part of the frequency spectrum. This feature seems to contradict

Langmuir probe measurements on CALTECH [4] where no definite radial propagation was seen. However, the two diagnostics measure different parts of the fluctuation wavelength spectrum. While for the CALTECH measurements the whole radial measurement range was 1.8 cm with a resolution of about 2 mm, the Li-beam is typically 1 cm in diameter. Thus, its sensitivity to structures having a poloidal size smaller than 1 cm is reduced. It is also important to note that our results show the characteristics of the fluctuations have a radial dependence, for example, at the LCFS there seems to be no propagation. Another important point is that this propagation can also be a projection of the poloidal movement of radially large structures.

From the present results it is not possible to determine if the perturbations always appear at the LCFS and travel outwards through the whole SOL, or whether they can also spontaneously appear everywhere in the SOL. Although outward propagation is always seen when the reference point of the τ–Z crosscorrelation function is placed in the SOL (see figure 10(a)), no correlation is evident between radial positions separated by more than $\approx$2 cm. This indicates either that the perturbations appear everywhere in the SOL or due to their poloidal movement they simply move out of (or into) the beam after travelling a few centimetres radially. To address this question a two-dimensional (2D) measurement, like the one outlined in [20], would be necessary.

Our results show that the position of the LCFS coincides with the position in the plasma where the electron density fluctuations have the shortest autocorrelation time and where the radial propagation of the perturbations changes sign. It is not clear whether this latter feature is connected with the well known fact that the poloidal propagation of the fluctuations also changes sign close to the LCFS.

In the SOL no significant negative correlation shows up between different radial positions. Therefore, the fluctuations in this region seem to be a response to changes in the edge plasma rather than to some rearrangement of the density profile in the SOL. However, the present accuracy of the reconstruction does not rule out the presence of some small-amplitude negative correlations in the SOL. The fluctuations inside the LCFS show more structure and definite negative correlations, and therefore it is more probable that some kind of instability causes a rearrangement of the density profile in this region. From the present experiments it is not clear whether the fluctuations in the SOL and in the edge plasma are manifestations of a single phenomenon, or independent of each other. To form a clearer picture of the processes involved, the accuracy of the measurements must be increased either by increasing the beam current (more light intensity) or by improving the detection efficiency.

Acknowledgments

The authors thank the W7-AS team for providing experimental data. Fruitful discussions with the fluctuation group and especially with Dr H Niedermeyer and Dr M Endler are acknowledged. Two of the authors (SZ and GK) would like to thank IPP-Garching for supporting this work both in Garching and Budapest.

References

[1] Wagner F and Stroth U 1985 *Plasma Phys. Control. Fusion* **35** 1321
[2] Liewer P C 1985 *Nucl. Fusion* **25** 543
[3] Wootton A J, Carreras B A, Matsumoto H, McGuire K, Peebles W A, Ritz Ch P, Terry P W and Zweben S J 1990 *Phys. Fluids* B **2** 2879

[4] Zweben S J and Gould R W 1985 *Nucl. Fusion* **25** 171
[5] Endler M, Niedermeyer H, Giannone L, Holzhauer E, Rudyj A, Theimer N, Tsois N and the ASDEX Team 1995 *Nucl. Fusion* **35** 1307
[6] Endler M, Giannone L, McCormick K, Niedermeyer H, Rudyj A, Theimer G, Tsois N and Zoletnik S 1995 *Phys. Scr.* **51** 610
[7] Komori A *et al* 1988 *Nucl. Fusion* **28** 1460
[8] Watts C *et al* 1996 *Phys. Plasmas* **3** 2013
[9] Fonck R J, Cosby G, Durst R D, Paul S F, Bretz N, Scott S, Synakowski E and Taylor G 1993 *Phys. Rev. Lett.* **70** 3736
[10] Sattler S, Hartfuss H J and the W7-AS Team 1994 *Phys. Rev. Lett.* **72** 653
[11] Callen J D 1992 *Phys. Fluids* B **4** 2142
[12] Fonck R J, Duperrex P A and Paul S F 1990 *Rev. Sci. Instrum.* **61** 3487
[13] Durst R D, Fonck R J, Cosby G, Evensen H and Paul S F 1992 *Rev. Sci. Instrum.* **63** 4907
[14] Evensen H, Brouchous D, Diebold D, Doczy M, Fonck R J and Nolan D 1992 *Rev. Sci. Instrum.* **63** 4928
[15] Komori A, Nagai S, Morisaki T and Kawai Y 1990 *Rev. Sci. Instrum.* **61** 3787
[16] Gianakon T A, Fonck R J, Callen J D, Durst R D, Kim J S and Paul S F 1992 *Rev. Sci. Instrum.* **63** 4931
[17] McCormick K, Fiedler S, Kocsis G, Schweinzer J and Zoletnik S 1996 *IPP-Garching Report* IPPIII/211
[18] McCormick K, Fiedler S, Kocsis G, Schweinzer J and Zoletnik S 1996 *Fusion Eng. Design* **34–35** 125
[19] Schweinzer J, Wolfrum E, Aumayr F, Pöckl M, Winter H, Schorn R P, Hintz E and Unterreiter A 1992 *Plasma Phys. Control. Fusion* **34** 1173
[20] Thomas D M 1996 *IEEE Trans. Plasma Sci.* **24** 27
[21] Zoletnik S and Kálvin S 1993 *Rev. Sci. Instrum.* **64** 1208
[22] Zoletnik S, Kocsis G, Fiedler S, McCormick K, Schweinzer J, Winter H P and the W7-AS Team 1996 *IPP-Garching Report* IPPIII/213
[23] Fonck R J, Ashley R, Durst R, Paul S F and Renda G 1992 *Rev. Sci. Instrum.* **63** 4924